Symmetric exclusion process under stochastic resetting

Urna Basu [1,*] Anupam Kundu,[2] and Arnab Pal[3,4,5]

[1]*Raman Research Institute, Bengaluru 560080, India*
[2]*International Centre for Theoretical Sciences, Tata Institute of Fundamental Research, Bengaluru 560089, India*
[3]*School of Chemistry, Raymond and Beverly Sackler Faculty of Exact Sciences, Tel Aviv University, Tel Aviv 6997801, Israel*
[4]*Center for the Physics and Chemistry of Living Systems, Tel Aviv University, 6997801, Tel Aviv, Israel*
[5]*Sackler Center for Computational Molecular and Materials Science, Tel Aviv University, 6997801, Tel Aviv, Israel*

We study the behavior of a symmetric exclusion process (SEP) in the presence of stochastic resetting where the configuration of the system is reset to a steplike profile with a fixed rate r. We show that the presence of resetting affects both the stationary and dynamical properties of SEPs strongly. We compute the exact time-dependent density profile and show that the stationary state is characterized by a nontrivial inhomogeneous profile in contrast to the flat one for $r = 0$. We also show that for $r > 0$ the average diffusive current grows linearly with time t, in stark contrast to the $\sqrt{t}$ growth for $r = 0$. In addition to the underlying diffusive current, we identify the resetting current in the system which emerges due to the sudden relocation of the particles to the steplike configuration and is strongly correlated to the diffusive current. We show that the average resetting current is negative, but its magnitude also grows linearly with time t. We also compute the probability distributions of the diffusive current, resetting current, and total current (sum of the diffusive and the resetting currents) using the renewal approach. We demonstrate that while the typical fluctuations of both the diffusive and reset currents around the mean are typically Gaussian, the distribution of the total current shows a strong non-Gaussian behavior.

I. INTRODUCTION

Stochastic resetting, which refers to intermittent interruption and restart of a dynamical process, has been a subject of immense interest in recent years. It has found applications in a wide range of areas starting from search problems [1–4], population dynamics [5,6], and enzymatic catalysis [7,8] to computer science [9,10], stock markets [11], and biological processes [12–14]. Stochastic resetting of a single Brownian particle is the paradigmatic example where the position of the particle is reset to a fixed point in space with a certain rate [15]. This simple act has drastic consequences on the statistical properties of the particle—it results in a nontrivial stationary state and anomalous relaxation behavior, as well as finite mean first passage time.

Several variations and extensions of this simple model have been explored in recent years [16–23]. Specific examples include resetting in the presence of an external potential [24,25], in a confinement [26,27], or to an extended region [28], and resetting to already excursed positions [29,30]. Stochastic resetting has also been studied in more general nonequilibrium contexts: in reaction processes [7,8], Lévy flights [31], coagulation-diffusion processes [32], telegraphic processes [33], for run-and-tumble particles [34], and to model nonequilibrium baths [35]. Studies were not only limited to a constant rate resetting; other protocols have also been investigated in great detail. These include deterministic

resetting [36], space- [37] or time-dependent [38,39] resetting rates, resetting followed by a refractory period [40,41], non-Markovian resetting [42–44], and resetting sensitive to internal dynamics [45].

An important question that naturally arises is how the presence of resetting dynamics affects the systems with many
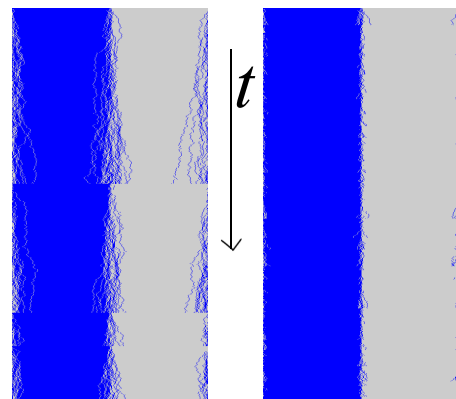
FIG. 1. Typical snapshots of time evolution of a system of size $L = 400$ for two different values of the resetting rate $r = 0.01$ (left) and $r = 0.1$ (right). The dark blue points indicate the presence of particles, and the light gray ones indicate empty sites. For a small value of r (left) the typical duration between two consecutive resetting events is longer, and the particles spread deeper into the empty half of the lattice, whereas for larger r (right) the resetting occurs more frequently and the density profile remains close to the steplike initial state.

*Corresponding author: urna@rri.res.in

interacting degrees of freedom. This issue has not been explored much so far except for a few handful of models. These studies include dynamics of KPZ-like fluctuating interfaces [46,47], one-dimensional quantum spin chains [48], and a pair of interacting Brownian particles [45,49]. In all these cases, resetting leads to nonequilibrium stationary states, characterized by non-Gaussian fluctuations. However, the effect of resetting on the behavior of current, which plays an important role in characterizing the nonequilibrium stationary state, has not been studied yet. This question is of paramount importance, because presence of stochastic resetting introduces an additional timescale and is expected to modify the behavior of current significantly. The exclusion processes [50], which are simple well-known models of interacting particles, provide a natural playground for exploring these questions.

In this article we study the effect of stochastic resetting on the symmetric exclusion process (SEP) [50,51] and explore how the presence of resetting changes the dynamical and stationary properties of SEPs. The stochastic resetting is implemented by interrupting the time evolution at some rate r and restarting the process from a specific configuration. It turns out that the incorporation of the resetting mechanism introduces an extra current J_{reset} in addition to the usual diffusive particle current J_{d}. We show that, for $r > 0$, the average diffusive current increases linearly with time t, in contrast to the $\sqrt{t}$ behavior in the absence of the resetting [52]. Additionally, the average resetting current also shows a linear temporal growth in magnitude, although it remains negative. We also compute the distribution of the diffusive current J_{d}, resetting current J_r, as well as the total current $J_r = J_{\text{d}} + J_{\text{reset}}$. We observe that, while the diffusive and resetting currents show Gaussian behavior, the fluctuations of the total current are characterized by a strongly non-Gaussian distribution.

The article is organized as follows: In the next section we define our system and summarize our main results. Section III is devoted to the computation of the time evolution of the density profile under resetting. In Sec. IV we investigate the behavior of the particle current; Secs. IV A and IV B focus on the diffusive and resetting currents, respectively, whereas the behavior of the total current J_r is explored in Sec. IV C. We conclude with some open questions in Sec. V.

II. MODEL AND RESULTS

The symmetric exclusion process (SEP) is a paradigmatic model for interacting particle systems [50,51] which has been used to describe a wide range of physical phenomena including particle transport in narrow channels, motion of molecular motors, ion transport through porous medium, etc. This process describes unbiased motion of particles on a lattice which interact via mutual local exclusion. In this section we define the dynamics of SEPs with stochastic resetting and present a brief summary of our main results.

Let us consider a periodic lattice of size L where each lattice site can contain at most one particle. The state of a site, say, x, is characterized by a variable s_x which takes values 1 and 0 depending on whether the site x is occupied or not, respectively. The configuration of the system is characterized by $\mathcal{C} = \{s_x; x = 0, 1, 2, \ldots, L-1\}$. We consider the case of

half-filling, i.e., the total number of particles $\sum_x s_x = \frac{L}{2}$. The system evolves according to the following two dynamical moves:

(1) *Hopping*: A particle randomly hops to one of its nearest neighboring sites with unit rate, provided the target site is empty.

(2) *Resetting*: In addition, the system is "reset" to some specific configuration $\mathcal{C}_0$ with rate r. In the following we consider $\mathcal{C}_0$ to be a steplike state where all the particles are in the left half of the lattice:

$$\mathcal{C}_0 := \begin{cases} s_x = 1 & \text{for } 0 \leqslant x \leqslant \frac{L}{2} - 1, \\ s_x = 0 & \text{otherwise.} \end{cases} \quad (1)$$

Both the hopping and resetting dynamics conserve the total number of particles, so that the half-filling condition is respected at all times, and the global particle density remains fixed at $1/2$. Between two resetting events the time evolution of the system is governed by the hopping dynamics only. The timescale associated with the resetting mechanism is given by r^{-1}, which also gives a measure of the typical duration between two consecutive resetting events. Figure 1 shows typical examples of the time evolution for two different values of the resetting rate r.

In the absence of resetting, the master equation governing the time evolution of the probability $\mathcal{P}_0(\mathcal{C}, t)$ for the system to be in the configuration $\mathcal{C}$ at time t is given by

$$\frac{d}{dt}\mathcal{P}_0(\mathcal{C}, t) = \mathcal{L}_0 \mathcal{P}_0(\mathcal{C}, t). \quad (2)$$

Here $\mathcal{L}_0$ is the Markov matrix in the absence of the resetting, i.e., $\mathcal{L}_0 \mathcal{P}_0(\mathcal{C}, t) = \sum_{\mathcal{C}'}[W_{\mathcal{C}' \to \mathcal{C}} \mathcal{P}_0(\mathcal{C}', t) - W_{\mathcal{C} \to \mathcal{C}'} \mathcal{P}_0(\mathcal{C}, t)]$ where $W_{\mathcal{C}' \to \mathcal{C}}$ denotes the rate for the jump $\mathcal{C} \to \mathcal{C}'$ due to hopping dynamics *only*. Note that, $W_{\mathcal{C}' \to \mathcal{C}} = 1$ only if the two configurations $\mathcal{C}$ and $\mathcal{C}'$ are connected by a single hop of a particle to a neighboring site.

Let $\mathcal{P}(\mathcal{C}, t)$ denote the probability of finding the system in the configuration $\mathcal{C}$ at time t in the presence of resetting. In this case, the master equation reads

$$\frac{d}{dt}\mathcal{P}(\mathcal{C}, t) = \mathcal{L}_0 \mathcal{P}(\mathcal{C}, t) + r \sum_{\mathcal{C}' \neq \mathcal{C}_0} \mathcal{P}(\mathcal{C}', t)\delta_{\mathcal{C}, \mathcal{C}_0}$$
$$- r\mathcal{P}(\mathcal{C}, t)(1 - \delta_{\mathcal{C}, \mathcal{C}_0})$$
$$= (\mathcal{L}_0 - r)\mathcal{P}(\mathcal{C}, t) + r\delta_{C, C_0}, \quad (3)$$

where $\delta_{\mathcal{C}, \mathcal{C}_0}$ is the Kronecker δ symbol, which takes the value unity when $\mathcal{C}$ is same as $\mathcal{C}_0$, and is zero otherwise. It is straightforward to write a formal solution of Eq. (3),

$$\mathcal{P}(\mathcal{C}, t) = e^{(\mathcal{L}_0 - r)t}\mathcal{P}(\mathcal{C}, 0) + r \int_0^t ds\, e^{(\mathcal{L}_0 - r)s}\delta_{C, C_0}$$
$$= e^{-rt}\mathcal{P}_0(\mathcal{C}, t) + r \int_0^t ds\, e^{-rs}\mathcal{P}_0(\mathcal{C}, s). \quad (4)$$

Here $\mathcal{P}_0(\mathcal{C}, t) = e^{\mathcal{L}_0 t}\mathcal{P}(\mathcal{C}, 0)$ is the probability of finding the system in configuration $\mathcal{C}$ at time t in the *absence of resetting* given that the system was initially at $\mathcal{C}_0$, i.e., $\mathcal{P}(\mathcal{C}, 0) = \mathcal{P}_0(\mathcal{C}, 0) = \delta_{\mathcal{C}, \mathcal{C}_0}$. Equation (4) is nothing but the renewal equation for the configuration probability, which has been obtained earlier and used to study resetting phenomena in various other contexts [15,46]. Note that Eq. (4) holds true irrespective of the specific choice of $\mathcal{C}_0$ given in Eq. (1).
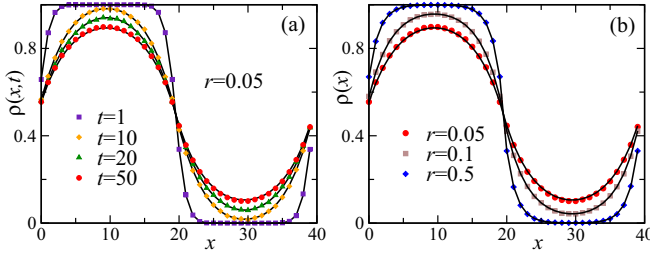
FIG. 2. Density profile: (a) Time evolution of the density profile $\rho(x,t)$, starting from a steplike initial condition, for resetting rate $r = 0.05$ and for different values of time t. The symbols correspond to the data obtained from numerical simulations, and the solid lines correspond to the analytical result [see Eq. (14)]. (b) The stationary density profile $\rho(x)$ for different reset rates r. The symbols correspond to the data obtained from numerical simulations, and the solid lines correspond to the analytical result [see Eq. (15)]. The lattice size $L = 40$ for both panels (a) and (b).

In the absence of resetting the ordinary SEP on a ring relaxes to an equilibrium state with flat density profile and zero current. The approach to the equilibrium state, starting from the steplike initial configuration $\mathcal{C}_0$, is characterized by a diffusive current flowing through the system. It has been shown that, for an infinitely large system, the time-integrated current measuring the net particle flux through the central bond up to time t grows as $\sqrt{t}$ for large t [52,53]. Presence of resetting is expected to affect these characteristics of SEPs which we investigate in detail in this paper. A brief summary of our results is presented below:

(1) First, we compute an exact expression for the evolution of the average density profile $\rho(x,t) = \langle s_x(t) \rangle$ for any arbitrary value of the resetting rate r, which is given in Eq. (10). We observe that the evolution is nontrivially modified due to the presence of resetting, which leads to an inhomogeneous stationary density profile [see Fig. 2(b)] in contrast to the flat one for $r = 0$.

(2) This inhomogeneous density profile provides some characterization of the nonequilibrium state of the system. It is, however, also important to look at how the particle currents in the system are affected by the introduction of resetting. In addition to the usual diffusive current $J_d(t)$ created due to the local hopping of the particles, there is also a contribution $J_{\text{reset}}(t)$ to the total current due to the global movements of the particles during the resetting events.

We show that the behavior of the diffusive current changes drastically in the presence of resetting. In particular, we compute the average diffusive current $\langle J_d(t) \rangle$ exactly, which, in the long-time limit, shows a linear growth with time t,

$$\langle J_d(t) \rangle \simeq t \sqrt{\frac{r}{r+4}}.$$

This behavior is in stark contrast to the $\sqrt{t}$ growth, which is seen in the absence of resetting [52]. Similar change in the dynamical behavior is also observed for the variance of the diffusive current, which also grows as $\sim t$ in the presence of resetting, as opposed to $\sqrt{t}$. We explore the behavior of the resetting current J_{reset} too and show that its average and variance also grow linearly with time. We also investigate

the probability distribution of $J_d(t)$ and demonstrate that, in the long-time regime, the typical fluctuations of $J_d(t)$ around its mean is characterized by a Gaussian distribution. Similar Gaussian fluctuations are also expected for the resetting current J_{reset}.

(3) Finally, we study the behavior of the total current $J_r = J_d + J_{\text{reset}}$ and calculate the average $\langle J_r(t) \rangle$ and the second moment $\langle J_r^2(t) \rangle$ as functions of time t. In the long-time limit the moments reach stationary values. In particular, we show that the average stationary current is given by

$$\langle J_r \rangle = \frac{1}{\sqrt{r(r+4)}}. \tag{5}$$

We also compute the stationary probability distribution of the total current $P_r^{\text{st}}(J_r)$, for small values of r, using a renewal approach. Interestingly, it turns out that this distribution is non-Gaussian and has very asymmetric behavior at the two tails.

III. DENSITY PROFILE

The presence of repeated resetting to the inhomogeneous configuration $\mathcal{C}_0$ destroys the translational invariance in the system and a nontrivial density profile can be expected, even in the stationary state. The average density $\rho(x,t) = \langle s_x(t) \rangle$ is given by the probability that the site x is occupied any time t. The time-evolution equation for the density profile can be derived by multiplying Eq. (3) by s_x and summing over all configurations $\mathcal{C}$,

$$\frac{d}{dt}\rho(x,t) = \rho(x+1,t) + \rho(x-1,t) - 2\rho(x,t)$$
$$- r\rho(x,t) + r\phi(x). \tag{6}$$

Here $\phi(x)$ is the density profile corresponding to the resetting configuration $\mathcal{C}_0$, which, as mentioned before, is also taken as the initial profile. The exact time-dependent density profile $\rho(x,t)$ can be obtained by solving Eq. (6). To this end we introduce the discrete Fourier transform

$$\tilde{\rho}(n,t) = \sum_{x=0}^{L-1} e^{i\frac{2\pi n x}{L}} \rho(x,t), \quad \text{with } n = 0, 1, 2, \ldots, L-1. \tag{7}$$

Substituting Eq. (7) in Eq. (6), we get

$$\frac{d}{dt}\tilde{\rho}(n,t) = -(\lambda_n + r)\tilde{\rho}(n,t) + r\tilde{\phi}(n) \tag{8}$$

with $\lambda_n = 2(1 - \cos\frac{2\pi n}{L})$ and $\tilde{\phi}(n)$ is the Fourier transform of the resetting (and initial) profile $\phi(x)$. Equation (8) can immediately be solved,

$$\tilde{\rho}(n,t) = \frac{r\tilde{\phi}(n)}{r+\lambda_n} + \frac{\lambda_n\tilde{\phi}(n)}{r+\lambda_n}e^{-(r+\lambda_n)t}. \tag{9}$$

The density profile is then obtained by inverting the Fourier transform,

$$\rho(x,t) = \frac{r}{L}\sum_{n=0}^{L-1}\frac{\tilde{\phi}(n)}{r+\lambda_n}e^{-i\frac{2\pi n x}{L}}$$
$$+ \frac{1}{L}\sum_{n=0}^{L-1}\frac{\lambda_n\tilde{\phi}(n)}{r+\lambda_n}e^{-(r+\lambda_n)t}e^{-i\frac{2\pi n x}{L}}. \tag{10}$$

In the stationary state, the second term decays exponentially, and the stationary density profile is given by

$$\rho(x) = \frac{r}{L} \sum_{n=0}^{L-1} \frac{\tilde{\phi}(n)}{r + \lambda_n} e^{-i\frac{2\pi n x}{L}} = \frac{1}{2} + \frac{r}{L} \sum_{n=1}^{L-1} \frac{\tilde{\phi}(n)}{r + \lambda_n} e^{-i\frac{2\pi n x}{L}},$$
(11)

where we have used the fact that $\tilde{\phi}(0) = \sum_x \phi(x) = L/2$. Clearly, in the absence of resetting, i.e., for $r = 0$, we get the flat profile which corresponds to the equilibrium scenario. For nonzero r, however, the stationary profile is nontrivial and corresponds to a nonequilibrium stationary state, carrying nonzero current. We will explore that in the next section.

It is worth mentioning that $\rho(x, t)$ also satisfies a renewal equation [following directly from Eq. (4)] in terms of the density profile $\rho_0(x, t)$ in the absence of resetting,

$$\rho(x, t) = e^{-rt} \rho_0(x, t) + r \int_0^t d\tau \, e^{-r\tau} \rho_0(x, \tau).$$
(12)

For the sake of completeness we have added a brief review of the density profile and its evolution for ordinary SEPs in Appendix A. Using the explicit form of $\rho_0(x, t)$ given in Eq. (A4) it is straightforward to check that Eq. (12) leads to Eq. (10).

We have not used any specific form of $\phi(x)$ so far; in fact, the results above are valid for resetting to any generic profile. For the specific choice of the steplike configuration given in Eq. (1) we have $\phi(x) = 1 - \Theta(x + 1 - \frac{L}{2})$ and

$$\tilde{\phi}(n) = \frac{1 - (-1)^n}{1 - e^{i\frac{2\pi n}{L}}} = \begin{cases} 1 + i \cot \frac{\pi n}{L} & \text{for odd } n \\ 0 & \text{for even } n \end{cases}.$$
(13)

In that case, the density profile takes the form

$$\rho(x, t) = \rho(x) + \frac{1}{L} \sum_{n=1,3}^{L-1} e^{-i\frac{2\pi n x}{L}} \frac{\lambda_n \left(1 + i \cot \frac{\pi n}{L}\right)}{r + \lambda_n} e^{-(r + \lambda_n)t},$$
(14)

where

$$\rho(x) = \frac{1}{2} + \frac{r}{L} \sum_{n=1,3}^{L-1} e^{-i\frac{2\pi n x}{L}} \frac{\left(1 + i \cot \frac{\pi n}{L}\right)}{r + \lambda_n}$$
(15)

is the stationary profile.

Figure 2(a) shows the time evolution of the density profile $\rho(x, t)$ for a specific resetting rate r, and Fig. 2(b) shows stationary profiles $\rho(x)$ for different values of r. In both cases, the analytical results (solid lines) are compared with the data obtained from numerical simulations (symbols). An excellent match confirms our analytical prediction.

IV. PARTICLE CURRENT

The behavior of current plays an important role in characterizing the interacting particle systems like exclusion processes. For ordinary SEPs, there is no particle current flowing through the system in the stationary (equilibrium) state. However, starting from a steplike initial configuration, the relaxation to equilibrium is characterized by the presence of a nonvanishing particle current. In particular, the behavior of the time-integrated current, i.e., the net particle flux through
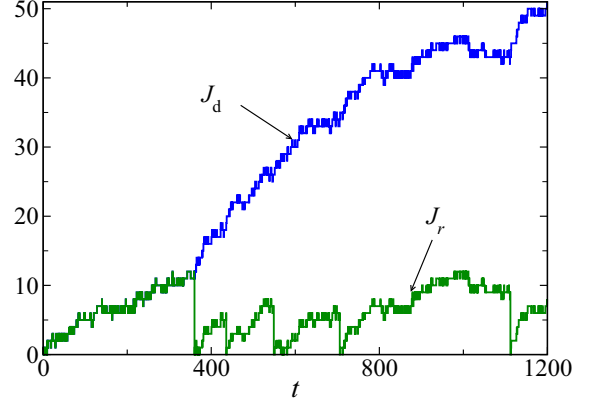
FIG. 3. Time evolution of the diffusive current $J_d(t)$ and the total current $J_r(t)$ along a typical trajectory of the system. On an average, the diffusive current increases with time t. The total current vanishes after each resetting event—indicated by the vertical lines on the light green curve—and reaches a stationary state in the long-time limit.

the central bond up to time t, has been studied extensively, and it was shown that at a long-time limit, the average flux grows $\sim \sqrt{t}$ [52,53].

In presence of resetting, there are two different kinds of particle motions; consequently the total current can be expressed as

$$J_r(t) = J_d(t) + J_{\text{reset}}(t).$$
(16)

Here J_d is net diffusive flux, i.e., the net number of particles which crossed the central bond due to the nearest-neighbor hopping. J_{reset} denotes the contribution due to the sudden reset to the steplike configuration $\mathcal{C}_0$. Note that, after a resetting, the system is brought back to $\mathcal{C}_0$, i.e., there are no particles to the right of the central bond, implying that the total current J_r is also reset to zero after each resetting event. Figure 3 shows the time evolution of J_d and J_r for a typical trajectory of the system. The sudden jumps in J_r indicate the resetting events.

In the absence of resetting, the only source of current is the diffusive hopping motion. In the following we explore the behaviors of all these three different currents, in the presence of resetting.

A. Diffusive current

The diffusive current $J_d(t)$ measures the total number of particles which crossed the central bond $(\frac{L}{2} - 1, \frac{L}{2})$ during the time interval $[0, t]$ and can be expressed as a time integral,

$$J_d(t) = \int_0^t ds \, j(s).$$
(17)

Here $j(t)$ denotes the instantaneous diffusive current, i.e., the number of particles crossing the central bond during the time interval t and $t + dt$. The average instantaneous current is given by

$$\langle j(t) \rangle = \left\langle s_{\frac{L}{2}-1} \left(1 - s_{\frac{L}{2}}\right) \right\rangle - \left\langle \left(1 - s_{\frac{L}{2}-1}\right) s_{\frac{L}{2}} \right\rangle$$
$$= \rho\left(\frac{L}{2} - 1, t\right) - \rho\left(\frac{L}{2}, t\right).$$
(18)
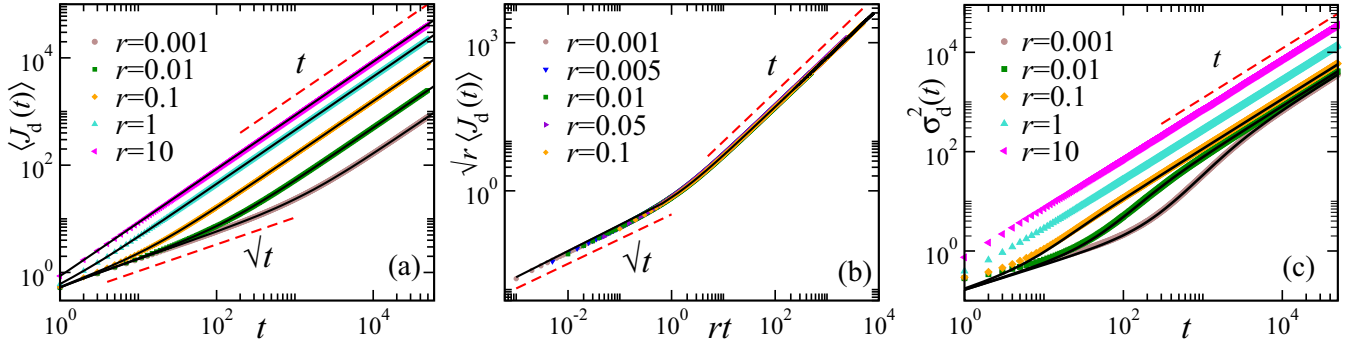
FIG. 4. Behavior of the diffusive current J_d. (a) Plot of $\langle J_d(t) \rangle$ as a function of time t for different values of r. The symbols correspond to the data obtained from numerical simulations, whereas the solid lines correspond to the analytical prediction [see Eq. (25)]. The lowermost curve corresponds to the smallest value of r. (b) Scaling collapse of $\sqrt{r}\langle J_d(t)\rangle$ for small r according to Eq. (27); the solid line corresponds to the predicted scaling function. (c) Plot of the variance $\sigma_d^2(t)$ vs t for different values of r. The curves corresponding to small values of r (three lower curves) are compared with the analytical predictions (solid lines). A lattice of size $L = 1000$ is used here for the numerical simulations.

Using the explicit expression for the density from Eq. (14) one gets

$$\langle j(t) \rangle = \frac{2}{L} \sum_{n=1,3}^{L-1} \left[\frac{r}{r+\lambda_n} + \frac{\lambda_n}{r+\lambda_n} e^{-(r+\lambda_n)t} \right]. \quad (19)$$

In the limit of thermodynamically large system size, i.e., $L \to \infty$, the sum in the above expression can be converted to an integral over the continuous variable $q = 2\pi n/L$, and we get

$$\langle j(t) \rangle = \int_0^{2\pi} \frac{dq}{2\pi} \left[\frac{r}{r+\lambda_q} + \frac{\lambda_q}{r+\lambda_q} e^{-(r+\lambda_q)t} \right] \quad (20)$$

where $\lambda_q = 2(1 - \cos q)$. In the long-time regime, the second term decays exponentially and $\langle j(t) \rangle$ reaches a stationary value,

$$\lim_{t \to \infty} \langle j(t) \rangle = \int_0^{2\pi} \frac{dq}{2\pi} \frac{r}{r+2(1-\cos q)} = \sqrt{\frac{r}{r+4}}. \quad (21)$$

The average net flux $\langle J_d(t) \rangle$ up to time t can be found by integrating the instantaneous current,

$$\langle J_d(t) \rangle = \sqrt{\frac{r}{r+4}}\, t + \int_0^{2\pi} \frac{dq}{2\pi} \frac{\lambda_q}{(r+\lambda_q)^2} (1 - e^{-(r+\lambda_q)t}). \quad (22)$$

Clearly, in the long-time regime, the second term goes to a constant, and the first term dominates the behavior of the average current which grows linearly with time,

$$\langle J_d(t) \rangle \simeq \sqrt{\frac{r}{r+4}}\, t. \quad (23)$$

This equation is one of our main results, which shows that the behavior of the diffusive current changes drastically by the presence of resetting; instead of the standard $\sqrt{t}$ growth in a diffusive system, resetting yields a much faster, linear, temporal growth of the diffusive current. The average current $\langle J_d(t) \rangle$ at any time t, i.e., before reaching the $\sim t$ behavior, can be obtained from Eq. (22) by evaluating the q integral numerically. In fact, one can also derive an alternative expression which lends itself more easily to numerical evaluation. Let us recall that the density profile $\rho(x,t)$ satisfies a renewal

equation (12) for any x. Then, clearly, $\langle j(t) \rangle$ must also satisfy the same renewal equation,

$$\langle j(t) \rangle = e^{-rt} \langle j_0(t) \rangle + r \int_0^t d\tau\, e^{-r\tau} \langle j_0(\tau) \rangle, \quad (24)$$

where $j_0(t)$ denotes the instantaneous current through the central bond in the absence of resetting. The average instantaneous current is given by $\langle j_0(t) \rangle = e^{-2t} I_0(2t)$ where I_0 is the modified Bessel function of the first kind (see Appendix B for details). The average diffusive net current is obtained by integrating the above equation w.r.t. time [see Eq. (17)],

$$\langle J_d(t) \rangle = \int_0^t d\tau\, e^{-r\tau} (1 + rt - r\tau) \langle j_0(\tau) \rangle. \quad (25)$$

It is straightforward to show that Eq. (25) is equivalent to Eq. (22). Average current $\langle J_d(t) \rangle$ computed from Eq. (25), for different values of r, is plotted together with the same obtained from simulation in Fig. 4(a).

An explicit form for $\langle J_d(t) \rangle$ can be derived for small $r \ll 1$. Using a variable transformation $w = r\tau$, and using the exact form for $\langle j_0(\tau) \rangle$, we get

$$\langle J_d(t) \rangle = \frac{1}{r} \int_0^{rt} dw (1 + rt - w) e^{-w} e^{-\frac{2w}{r}} I_0\left(\frac{2w}{r} \right). \quad (26)$$

For small r, the argument of I_0 is large, and one can use the asymptotic form for the modified Bessel function given in Eq. (B5),

$$\langle J_d(t) \rangle \simeq \frac{1}{r} \int_0^{rt} dw (1 + rt - w) e^{-w} \frac{1}{2\sqrt{\pi w/r}}$$
$$= \frac{1}{2\sqrt{r}} \left[\left(rt + \frac{1}{2} \right) \mathrm{erf}(\sqrt{rt}) + \sqrt{\frac{rt}{\pi}} e^{-rt} \right]. \quad (27)$$

In the short time-regime this function grows as $\sqrt{t}$, which is reminiscent of the free SEP and crosses over to the linear behavior for $t \gg r^{-1}$. Figure 4(b) shows plot of $\sqrt{r}\langle J_d(t) \rangle$ as a function of rt for different small values of r, which shows a perfect collapse and matches the scaling function given by the above equation.

To characterize the fluctuation of the diffusive current we next calculate the second moment of J_d. The above renewal

equation method cannot be applied directly to compute higher order moments. To this end, we now adopt a different approach. Let us assume that there are n resetting events during the time interval $[0, t]$; moreover, let t_i denote the interval between $(i-1)$th and ith events, so that $\sum_{i=1}^{n+1} t_i = t$. Note that, t_{n+1} denotes the time interval between the last reset and the final time t. Let us also recall that between two consecutive resetting events the system evolves following ordinary SEP dynamics. The diffusive current during the interval $[0, t]$ can then be expressed as

$$J_{\rm d} = \sum_{i=1}^{n+1} J_0(t_i), \qquad (28)$$

where $J_0(t_i)$ are independent of each other. For notational convenience, we denote $J_i \equiv J_0(t_i)$. The probability density that the diffusive current will have a value $J_{\rm d}$ in time t is then given by

$$P(J_{\rm d}, t) = \sum_{n=0}^{\infty} \int_0^t \prod_{i=1}^{n+1} dt_i \mathcal{P}_n(\{t_i\}; t) \\ \times \int \prod_{i=1}^{n+1} dJ_i P_0(J_i, t_i) \delta \left(J_{\rm d} - \sum_i J_i \right),$$

where

$$\mathcal{P}_n(\{t_i\}; t) = r^n e^{-r \sum_{i=1}^{n+1} t_i} \delta \left(t - \sum_i t_i \right) \qquad (29)$$

denotes the probability of having n resetting events with duration t_i within the interval $[0, t]$. The distribution of the individual J_i are denoted by $P_0(J_i, t_i)$, which is exactly the distribution of the diffusive current in SEPs, in the absence of resetting.

To handle the constraints presented by the δ functions, it is convenient to calculate the Laplace transform w.r.t. time t of the moment-generating function $\langle e^{\lambda J_{\rm d}} \rangle$,

$$Q(s, \lambda) = \mathcal{L}_{t \to s}[\langle e^{\lambda J_{\rm d}} \rangle] = \int_0^{\infty} dt e^{-st} \langle e^{\lambda J_{\rm d}} \rangle \\ = \int_0^{\infty} dt e^{-st} \int dJ_{\rm d} e^{\lambda J_{\rm d}} P(J_{\rm d}, t). \qquad (30)$$

Using Eq. (29), and performing the integrals over $J_{\rm d}$ and t, we get

$$Q(s, \lambda) = \sum_{n=0}^{\infty} r^n \int_0^{\infty} \prod_i^{n+1} dt_i \exp \left[-(r+s) \sum_{i=1}^{n+1} t_i \right] \\ \times \int \prod_i^{n+1} dJ_i \exp \left[\lambda \sum_{i=1}^{n+1} J_i \right] P_0(J_i, t_i) \\ = \sum_{n=0}^{\infty} r^n h(s, \lambda)^{n+1}, \qquad (31)$$

where we have denoted

$$h(s, \lambda) = \int_0^{\infty} d\tau e^{-(r+s)\tau} \int dJ_0 e^{\lambda J_0} P_0(J_0, \tau). \qquad (32)$$

Performing the sum in Eq. (31), we get

$$Q(s, \lambda) = \frac{h(s, \lambda)}{1 - rh(s, \lambda)}, \qquad (33)$$

which gives a simple relation between the moment-generating functions of the current in the presence and absence of resetting. To calculate $h(s, \lambda)$ we need the current distribution $P_0(J_0, \tau)$ for the ordinary SEP, which is not known in general for arbitrary values of τ. However, for small values of r and s, the τ integral in Eq. (32) is dominated by large values of τ, and in that case one can use the result of Ref. [52] where the authors have derived an expression for the moment-generating function of $J_0(\tau)$ in the large time limit. Adapting their result to our specific case (see Appendix B 1 for details), we have

$$\int dJ_0 e^{\lambda J_0} P_0(J_0, \tau) = \langle e^{\lambda J_0} \rangle \simeq e^{\sqrt{\tau} F(\lambda)}, \qquad (34)$$

with

$$F(\lambda) = -\frac{1}{\sqrt{\pi}} \text{Li}_{3/2}(1 - e^{\lambda}). \qquad (35)$$

Here $\text{Li}_{\alpha}(z)$ denotes the Poly-Logarithm function [see Ref. [54], Eq. (25.12.10)]. Substituting Eq. (34) in Eq. (32) and performing the integral over τ, we get, for small r and s,

$$h(s, \lambda) = \frac{1}{r+s} \left[1 + \frac{\sqrt{\pi} F(\lambda)}{2\sqrt{r+s}} e^{\frac{F(\lambda)^2}{4(r+s)}} \left(1 + \text{erf} \left[\frac{F(\lambda)}{2\sqrt{r+s}} \right] \right) \right]. \qquad (36)$$

One can easily extract the Laplace transforms of the moments using Eq. (36) along with (33). First, we have

$$\mathcal{L}_{t \to s}[\langle J_{\rm d}(t) \rangle] = \frac{d}{d\lambda} Q(s, \lambda) \Big|_{\lambda=0} = \frac{\sqrt{r+s}}{2s^2}. \qquad (37)$$

The average current can be obtained by inverting the Laplace transform,

$$\mu_d(t) \equiv \langle J_{\rm d}(t) \rangle = \mathcal{L}_{s \to t}^{-1} \left[\frac{\sqrt{r+s}}{2s^2} \right]. \qquad (38)$$

The inversion can be performed exactly using Mathematica and yields

$$\mu_d(t) = \frac{1}{2\sqrt{r}} \left[\left(rt + \frac{1}{2} \right) \text{erf}(\sqrt{rt}) + \sqrt{\frac{rt}{\pi}} e^{-rt} \right]. \qquad (39)$$

Note that the above equation is the same as Eq. (27), which was obtained using a different method.

The Laplace transform of the second moment is obtained from the second derivative of $Q(s, \lambda)$,

$$\mathcal{L}_{t \to s} \langle J_{\rm d}^2(t) \rangle = \frac{d^2}{d\lambda^2} Q(s, \lambda) \Big|_{\lambda=0} = \frac{1}{\pi s^2} + \frac{b\sqrt{r+s}}{2s^2} + \frac{r}{2s^3}, \qquad (40)$$

where $b = (1 - 1/\sqrt{2})$. Fortunately, the inverse Laplace transform can be performed exactly in this case also, and it yields, for small r,

$$\langle J_{\rm d}^2(t) \rangle = \frac{1}{4\pi} \left[t(\pi rt + 4) + 2b\sqrt{\pi} t e^{-rt} \\ + \frac{b\pi}{\sqrt{r}} (1 + 2rt) \text{erf}(\sqrt{rt}) \right]. \qquad (41)$$
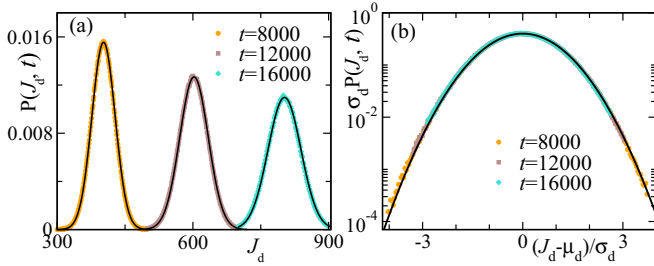
FIG. 5. Distribution of the diffusive current $P(J_d, t)$ for $r = 0.01$: (a) Plot of $P(J_d, t)$ vs J_d for different values of t, the leftmost curve corresponding to the smallest value of t. The solid lines correspond to the predicted Gaussian form (43). (b) The same data are plotted as a function of $(J_d - \mu_d)/\sigma_d$. The solid black line corresponds to a standard normal distribution $\mathcal{N}(0, 1)$.

Note that the above expression is expected to be valid for large t, as we have assumed s to be small. The variance of the diffusive current $\sigma_d^2(t) = \langle J_d^2(t) \rangle - \langle J_d(t) \rangle^2$ can be obtained using Eqs. (39) and (41). In particular, in the long-time limit, the variance increases linearly with time t and is given by

$$\sigma_d^2(t) \simeq t \left[\frac{4 - \pi}{4\pi} + \frac{\sqrt{r}}{2} \left(1 - \frac{1}{\sqrt{2}} \right) \right]. \quad (42)$$

Figure 4(c) shows a plot of $\sigma_d^2(t)$ versus t for different values of r, obtained from numerical simulations; all the curves show linear growth in the long-time regime. The curves corresponding to small values of $r \ll 1$ are compared with the analytical result (solid lines), which shows a perfect match for $t > 10$.

Distribution of J_d: It is interesting to investigate the probability distribution of the diffusive current $J_d(t)$. From Eq. (28) we observe that $J_d(t)$ is the sum of the hopping currents $J_0(t_i)$ between successive resetting events. Since the time evolution of the system is Markovian and after each resetting event the system is brought back to the initial configuration, the variables $J_0(t_i)$ are independent and distributed identically [55]. As mentioned earlier, the distribution of $J_0(t_i)$ is known [52] and has finite moments. Over a large time interval t, the number n of resetting events, which is also a random quantity, is typically large and on an average grows linearly with time t; in fact, $\langle n \rangle = rt$. For $t \gg r^{-1}$, $J_d(t)$ is a sum of a large number of independent random variables. Hence, by the central limit theorem, one can expect that for large t, the typical distribution of J_d would be a Gaussian:

$$P(J_d, t) \simeq \frac{1}{\sqrt{2\pi \sigma_d^2(t)}} \exp \left\{ -\frac{[J_d - \mu_d(t)]^2}{2\sigma_d^2(t)} \right\}, \quad (43)$$

where the mean $\mu_d(t)$ and the variance $\sigma_d^2(t)$ are given in Eqs. (39) and (42), respectively. This prediction is verified in Fig. 5(a) where the Gaussian form of $P(J_d, t)$ is compared to the data obtained from numerical simulations for a set of (large) values of t and fixed r. Clearly, the analytical curves are indistinguishable from the simulation data, which confirms our prediction. Figure 5(b) shows the same data plotted against the scaled variable $[J_d - \mu_d(t)]/\sigma_d(t)$ and compared with the standard normal distribution (solid black line).

B. Resetting current

The presence of the resetting dynamics gives rise to a resetting current J_{reset} [see Eq. (16)], which measures the flow of particles due to the sudden change in the configuration of the system. In this section we investigate the properties of this resetting current. Let us remember that the number of particles crossing the central bond (from right to left) at the resetting event is exactly same as the hopping current (from left to right) during the period after the previous resetting event. The net resetting current during a time interval $[0, t]$ then can be expressed as

$$J_{\text{reset}} = -\sum_{i=1}^{n} J_0(t_i), \quad (44)$$

where, as before, n denotes the number of resetting events in time t and t_i denotes the interval between the $(i - 1)$th and ith resetting events. Note that the upper limit of the sum is n in Eq. (44) as there is no contribution to the resetting current after the last resetting event.

To calculate the moments of J_{reset} we follow the same method as in Sec. IV A and calculate the Laplace transform of the moment-generating function of J_{reset},

$$K(s, \lambda) = \int_0^\infty dt \, e^{-st} \int dJ_{\text{reset}} e^{\lambda J_{\text{reset}}} \mathscr{P}(J_{\text{reset}}, t). \quad (45)$$

Here $\mathscr{P}(J_{\text{reset}}, t)$ denotes the probability that the resetting current has a value J_{reset} at time t and is given by

$$\mathscr{P}(J_{\text{reset}}, t) = \sum_{n=0}^\infty \int_0^t \prod_{i=1}^{n+1} dt_i \mathcal{P}_n(\{t_i\}; t)$$
$$\times \int \prod_{i=1}^{n} dJ_i P_0(J_i, t_i) \delta \left(J_{\text{reset}} + \sum_{i=1}^{n} J_i \right), \quad (46)$$

with $\mathcal{P}_n(\{t_i\}; t)$ given in Eq. (29). As before, we have used $J_i \equiv J_0(t_i)$. Using Eq. (46) in Eq. (45) and performing the integrals over t and J_{reset}, we get

$$K(s, \lambda) = \frac{1}{(r + s)} \sum_{n=0}^\infty r^n h(s, -\lambda)^n$$
$$= \frac{1}{(r + s)[1 - rh(s, -\lambda)]}, \quad (47)$$

where $h(s, \lambda)$ is given by Eq. (32). As mentioned already, it can computed exactly for small values of r, s and is given by Eq. (36).

Next we calculate the moments of the resetting current using Eqs. (47) along with Eq. (36). First, we have the Laplace transform of the average resetting current,

$$\mathcal{L}_{t \to s}[\langle J_{\text{reset}}(t) \rangle] = \frac{d}{d\lambda} K(s, \lambda) \bigg|_{\lambda = 0} = -\frac{r}{2s^2 \sqrt{r + s}}. \quad (48)$$

The inverse transform can be performed exactly to obtain

$$\langle J_{\text{reset}}(t) \rangle = -\frac{1}{2\sqrt{r}} \left[\left(rt - \frac{1}{2} \right) \text{erf}(\sqrt{rt}) + \sqrt{\frac{rt}{\pi}} e^{-rt} \right]. \quad (49)$$

Note that the above expression is expected to be valid for small values of $r \ll 1$ and large $t \gg 1$. Equation (49) is very
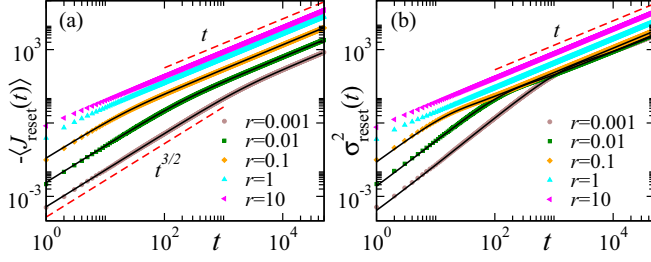
FIG. 6. Behavior of the resetting current J_{reset}: (a) Plot of $-\langle J_{\text{reset}}(t)\rangle$ as a function of time for different values of r obtained from numerical simulations. The lowermost curve corresponds to the smallest value of r. The black solid lines correspond to the analytical prediction (49) for small values of r. (b) Variance of the resetting current $\sigma^2_{\text{reset}}(t)$ as a function of time t for different values of r. The curves corresponding to small values of r (three lower curves) are compared with the analytical result (black solid lines). A lattice of size $L = 1000$ is used for all the numerical simulations.

similar to Eq. (39), which gives the average diffusive current $\langle J_{\text{d}}(t)\rangle$, except, of course, the fact that the average resetting current is negative. In fact, at very long times $t \gg r^{-1}$, we see a linear growth in magnitude,

$$\langle J_{\text{reset}}(t)\rangle = -\langle J_{\text{d}}(t)\rangle \simeq -\frac{\sqrt{r}t}{2}. \quad (50)$$

At short times, however, a different behavior is seen. From Eq. (49), for $t \ll r^{-1}$, we have

$$\langle J_{\text{reset}}(t)\rangle = -\frac{2rt^{3/2}}{3\sqrt{\pi}} + O(t^{5/2}). \quad (51)$$

Clearly, at short times, the resetting current grows much faster than the diffusive current. Figure 6(a) shows a plot of $\langle J_{\text{reset}}(t)\rangle$ as a function of t for different values of r which illustrates these features.

It is also interesting to look at the fluctuations of J_{reset}. From Eq. (47) we can find the Laplace transform of the second moment,

$$\mathcal{L}_{t \to s}\left[\langle J^2_{\text{reset}}(t)\rangle\right] = \frac{d^2}{d\lambda^2}K(s,\lambda)\bigg|_{\lambda=0}$$
$$= \frac{br}{2s^2\sqrt{r+s}} + \frac{r(\pi r + 2s)}{2\pi s^3(r+s)}, \quad (52)$$

where, as before, we have used $b = 1 - \frac{1}{\sqrt{2}}$. Once again, the Laplace transform can be inverted exactly and yields, for $r \ll 1$ and $t \gg 1$,

$$\langle J^2_{\text{reset}}(t)\rangle = \frac{1}{4\pi r}[2e^{-rt}(2 - \pi + br\sqrt{\pi t}) + \pi - r + 4rt$$
$$+ \pi(rt-1)^2 + b\pi\sqrt{r}(2rt-1)\text{erf}(\sqrt{rt})]. \quad (53)$$

The variance of the resetting current $\sigma^2_{\text{reset}}(t) = \langle J^2_{\text{reset}}(t)\rangle - \langle J_{\text{reset}}(t)\rangle^2$ can be computed from Eqs. (53) and (49), and it turns out that the variance also increases linearly at the long-time limit $t \gg r^{-1}$. In fact, it is straightforward to show that, in this limit, $\sigma^2_{\text{reset}}(t) = \sigma^2_d(t)$ [see Eq. (42)]. Figure 6(b) shows $\sigma^2_{\text{reset}}(t)$ for different values of r obtained from numerical simulations together with the analytical prediction for small r.

We conclude the discussion about the resetting current with a brief comment about the probability distribution $\mathscr{P}(J_{\text{reset}}, t)$. Since J_{reset}, similar to J_{d}, is also a sum of a set of independent variables $J_0(t_i)$, we can use the central limit theorem to predict the behavior of the corresponding distribution. In fact, for $rt \gg 1$, one can expect that $\mathscr{P}(J_{\text{reset}}, t)$ is similar to $P(J_{\text{d}}, t)$ and has a Gaussian behavior around the mean value,

$$\mathscr{P}(J_{\text{reset}}, t) \simeq \frac{1}{\sqrt{2\pi\sigma^2_{\text{reset}}(t)}} \exp\left\{-\frac{[J_{\text{reset}} - \langle J_{\text{reset}}(t)\rangle]^2}{2\sigma^2_{\text{reset}}(t)}\right\}.$$

C. Total current

In this section we investigate the behavior of the total current J_r, as defined in Eq. (16). $J_r(t)$ measures the net number of particles which have crossed the central bond towards the right (by hopping, or due to resetting) up to time t. As already mentioned, J_r is set to zero after every resetting event; the contribution to the total current comes only from the diffusion of the particles after the last resetting event. Consequently, one can write a renewal equation for $P_r(J_r, t)$, the probability that, at time t, the total current will have a value J_r,

$$P_r(J_r, t) = e^{-rt}P_0(J_r, t) + r\int_0^t ds\, e^{-rs}P_0(J_r, s). \quad (54)$$

Here $P_0(J_r, s)$ denotes the probability that, starting from $\mathcal{C}_0$, in the absence of resetting, J_r number of particles cross the central bond until time s. We will use the above equation to explore $P_r(J_r, t)$, but, first it is useful to investigate the mean and the variance of the total current.

It is easy to see that all moments of J_r should also satisfy a renewal equation similar to Eq. (54). In particular, the average total current must satisfy

$$\langle J_r(t)\rangle = e^{-rt}\langle J_0(t)\rangle + r\int_0^t d\tau\, e^{-r\tau}\langle J_0(\tau)\rangle, \quad (55)$$

where $\langle J_0(t)\rangle$ is the average current in the absence of resetting and is given by Eq. (B4). Unfortunately, the above integral in Eq. (55) cannot be computed analytically. However, it is possible to numerically evaluate the integral and get $\langle J_r(t)\rangle$ for any time t. This is shown in Fig. 7 for different values of r and compared with numerical simulations (symbols) which match perfectly at all times.

For small values of r, a more explicit expression for the average total current $\langle J_r(t)\rangle$ can be derived. In that case, it is convenient to rewrite Eq. (55) as

$$\langle J_r(t)\rangle = e^{-rt}\langle J_0(t)\rangle + \int_0^{rt} du\, e^{-u}\left\langle J_0\left(\frac{u}{r}\right)\right\rangle. \quad (56)$$

The integral is dominated by the contribution from small $u \sim O(1)$; consequently, u/r is large for small r, and we can use the asymptotic expression $\langle J_0(u/r)\rangle \simeq \sqrt{u/r\pi}$. Substituting that in the above equation, and performing the integral, we get, for large t,

$$\langle J_r(t)\rangle = \frac{1}{2\sqrt{r}}\text{erf}(\sqrt{rt}). \quad (57)$$

Equation (57) provides an explicit expression for the average total current for small r and in the large time regime. Note that $\langle J_r(t)\rangle$ given by the above equation is the same as $\langle J_{\text{d}}(t)\rangle +$
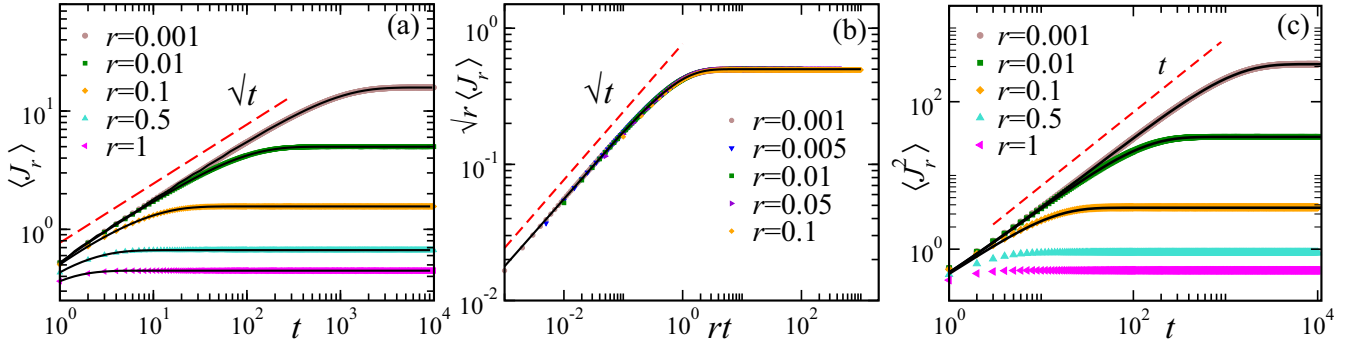
FIG. 7. Behavior of the total current J_r: (a) Plot of average total current $\langle J_r(t) \rangle$ as a function of time for different values of r, with the uppermost curve corresponding to the smallest value of r. Solid lines and symbols correspond to the analytical result and data from numerical simulations, respectively. (b) Plot of $\sqrt{r}\langle J_r(t) \rangle$ as a function of the scaled variable rt, for small values of r. The solid line corresponding to the scaling function $\mathrm{erf}(\sqrt{rt})/2$ [see Eq. (57)]. (c) Second moment of the total current $\langle J_r^2(t) \rangle$ as a function of time t for different values of r. The curves corresponding to small values of r (three upper curves) are compared with the analytical result (61) (solid lines). A lattice of size $L = 1000$ is used for all the numerical simulations.

$\langle J_{\text{reset}}(t) \rangle$, as clearly seen from Eqs. (39) and (49). This is expected as the total current is a sum of the diffusive current and the resetting current [see Eq. (16)].

We have also measured the total current J_r from numerical simulations. Figure 7(b) shows a plot of $\sqrt{r}\langle J_r(t) \rangle$ as a function of rt for different (small) values of r, as obtained from numerical simulation; the solid line corresponds to $\mathrm{erf}(\sqrt{rt})$. The perfect collapse of all the curves verifies our analytical prediction.

From Eq. (57) it can be seen that for $t \ll r^{-1}$ the average total current grows as $\sqrt{t}$, which is a signature of the ordinary SEP. On the other hand, in the large time limit $\langle J_r \rangle$ reaches a stationary value $1/2\sqrt{r}$.

In fact, the stationary value of the average total current $\langle J_r \rangle$ can be calculated exactly from Eq. (55) for any value of r. As we have already seen, at large times t, $\langle J_0(t) \rangle \sim \sqrt{t}$, hence, the first term in Eq. (55) decays exponentially and the large-time behavior of the average total current is dominated by the second integral in the above equation. Recalling Eq. (B4) and using the series expansion of the modified Bessel functions I_0 and I_1 [see Ref. [54], Eq. (10.25.2)] we have

$$\int_0^t d\tau e^{-r\tau} \langle J_0(\tau) \rangle$$

$$= \sum_{m=0}^{\infty} \frac{1}{m!(m+1)!} \frac{1}{(r+2)^{2m+3}} (\Gamma_{2m+3} - \Gamma_{2m+3}[(r+2)t]$$

$$+ (r+2)(m+1)\{\Gamma_{2m+2} - \Gamma_{2m+2}[(r+2)t]\}), \quad (58)$$

where Γ_n and $\Gamma_n(x)$ are the gamma function and the incomplete gamma function, respectively. $\Gamma_n(x)$ decays to zero for large x for all values of n, and hence, in the long-time limit we have the contributions only from the t-independent terms,

$$\lim_{t \to \infty} \langle J_r \rangle \simeq r \sum_{m=0}^{\infty} \frac{(2m+1)!}{m!(m+1)!} \frac{(m+1)(r+2) + 2m + 2}{(r+2)^{2m+3}}$$

$$= \frac{1}{\sqrt{r(r+4)}}. \quad (59)$$

Clearly, in the long-time limit the average total current reaches a stationary value $\mu_r = 1/\sqrt{r(r+4)}$ which decreases as the

resetting rate r is increased. For small r, $\mu_r \approx \frac{1}{2\sqrt{r}}$ which is same as what we obtained by taking $t \to \infty$ limit in Eq. (57). On the other hand, for large $r \gg 1$, μ_r approaches $1/r$.

Physically, the limiting behaviors of the stationary value of the average total current can be understood from the following argument. Since the value of J_r is reset to zero after each resetting event, the final contribution to J_r comes only from the diffusion of particles after the last resetting event. Moreover, the typical duration since the last resetting event is $\tau_r \sim 1/r$. For small r, this typical duration is long, and the average diffusive current (without resetting) during this period is $\sim \sqrt{\tau_r} = 1/\sqrt{r}$. On the other hand, for large r, τ_r is small, and the diffusive current is $\sim \tau_r = 1/r$.

Next we calculate the second moment of the total current $\langle J_r(t)^2 \rangle$. As mentioned already, the second moment also satisfies a renewal equation of the form

$$\langle J_r(t)^2 \rangle = e^{-rt} \langle J_0^2(t) \rangle + r \int_0^t d\tau e^{-r\tau} \langle J_0^2(\tau) \rangle. \quad (60)$$

The above equation is valid at all times and for all values of r. Unfortunately, however, the behavior of $\langle J_0^2(\tau) \rangle$ is known only for long-time τ [see Eq. (B7)], so we are not able to calculate an exact analytical expression for $\langle J_r(t)^2 \rangle$ for any arbitrary time t. Nevertheless, one can use Eq. (60) along with Eqs. (B6) and (B7) to calculate $\langle J_r(t)^2 \rangle$ for small values of r, where the integral in Eq. (60) is dominated by the contribution from large $\tau \gg r^{-1}$. This exercise leads to a simple analytical formula for the second moment for small r (and large time t),

$$\langle J_r^2(t) \rangle \simeq \frac{1}{\pi r}(1 - e^{-rt}) + \frac{1}{2\sqrt{r}}\left(1 - \frac{1}{\sqrt{2}}\right)\mathrm{erf}(\sqrt{rt}). \quad (61)$$

Figure 7(c) shows the plot of $\langle J_r^2(t) \rangle$ as a function of t for different values of r. The curves for small r are compared with the analytical result Eq. (61), which show an excellent match. Similar to the average total current, the second moment $\langle J_r^2(t) \rangle$ also eventually reaches a stationary value which, for small values of r, can be obtained by taking $\lim t \to \infty$ in Eq. (61),

$$\langle J_r^2 \rangle = \frac{1}{\pi r} + \frac{1}{2\sqrt{r}}\left(1 - \frac{1}{\sqrt{2}}\right). \quad (62)$$

One can immediately calculate the stationary value of the variance $\sigma_r^2 = \langle J_r^2 \rangle - \langle J_r \rangle^2$; as $r \to 0$, $\sigma_r^2 \simeq (4 - \pi)/4\pi r$.

On the other hand, for short-time t, we have

$$\langle J_r^2(t) \rangle \simeq \frac{t}{\pi} + \sqrt{\frac{t}{\pi}}\left(1 - \frac{1}{\sqrt{2}}\right). \quad (63)$$

At very short times, one expects a $\sqrt{t}$ behavior which crosses over to a linear behavior as t is increased. This is also seen in Fig. 7(c), where the approach to the stationary value appears predominantly linear.

Correlation between J_d and J_{reset}: The computation of the second moment of the total current J_r provides a way to estimate the correlation between the diffusive and resetting components of the current. From the definition of the total current (16), we get

$$\langle J_r^2(t) \rangle = \langle J_d^2(t) \rangle + \langle J_{\text{reset}}^2(t) \rangle + 2\langle J_d(t)J_{\text{reset}}(t) \rangle. \quad (64)$$

The connected correlation $C(t) = \langle J_d(t)J_{\text{reset}}(t) \rangle - \langle J_d(t) \rangle \langle J_{\text{reset}}(t) \rangle$ is then given by

$$C(t) = \frac{1}{2}\left[\sigma_r^2(t) - \sigma_d^2(t) - \sigma_{\text{reset}}^2(t)\right], \quad (65)$$

where σ_r^2, σ_d^2, and σ_{reset}^2 are the variances of the total, diffusive, and resetting currents, respectively. Using Eqs. (61), (41), and (53) along with Eqs. (57), (39), and (49), we get, for small values of r,

$$C(t) = \frac{1}{4\pi r}\Bigg(4 - \pi + rte^{-2rt}$$
$$+ e^{-rt}\{\pi - 4 - 2r\sqrt{\pi t}[b - \sqrt{rt}\,\text{erf}(\sqrt{rt})]\}$$
$$- rt(4 - \pi + \pi rt) - b\pi\sqrt{r}(2rt - 1)\text{erf}(\sqrt{rt})$$
$$+ \pi\left(r^2t^2 - \frac{1}{4}\right)\text{erf}(\sqrt{rt})^2\Bigg). \quad (66)$$

Clearly, the diffusive and resetting currents are strongly correlated. To understand the nature of this correlation we look at the limiting behavior of $C(t)$. At long times $t \gg r^{-1}$, we get a linear temporal growth from Eq. (66),

$$C(t) \simeq -\sigma_d^2(t) \simeq -t\left[\frac{4 - \pi}{4\pi} + \frac{b\sqrt{r}}{2}\right]. \quad (67)$$

On the other hand, for short times $t \ll r^{-1}$ (but $t \gg 1$) we get

$$C(t) = -\frac{2br}{3\sqrt{\pi}}t^{3/2} + O(t^2). \quad (68)$$

In fact, the correlation remains negative at all times. Figure 8 shows a plot of $-C(t)$ versus t for different values of r obtained from numerical simulations (symbols) along with the analytical prediction (solid lines) for small values of r.

The presence of a nontrivial correlation between the diffusive and resetting currents suggests that even though the fluctuations of both these components of current are Gaussian in nature, the distribution of the total current need not be so. In the following we investigate this issue and show that, indeed, the fluctuations of J_r are characterized by a strongly non-Gaussian distribution.

Probability distribution of J_r: In this section we explore the behavior of the probability distribution of the total current $P_r(J_r, t)$ using the renewal equation (54). In the absence of
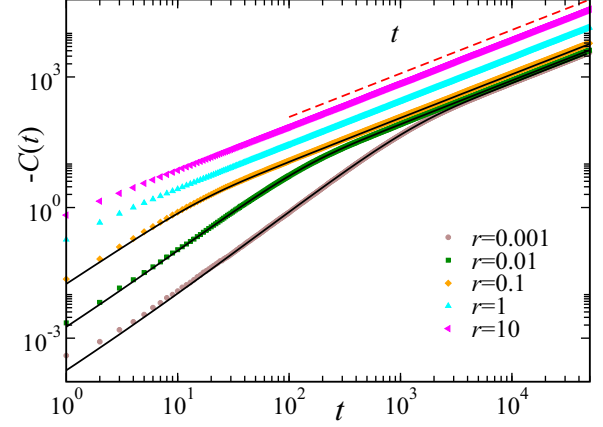
FIG. 8. Correlation between diffusive and resetting currents: Plot of $-C(t)$ as a function of time t for different values of r; the lowest curve corresponds to the smallest value of r. The data from the numerical simulations (symbols) are compared to the analytical prediction from Eq. (66) (solid lines) for small values of r. Lattice size $L = 1000$ is used for the simulations.

resetting, the fluctuations of the total (diffusive) current are characterized by a Gaussian distribution in the long-time limit (see Appendix B 1 for more details). Using the Gaussian form of $P_0(J_r, t)$ one can calculate the total current distribution $P_r(J_r, t)$ for small values of r (for small r the integral is dominated by the large t contribution). It is particularly interesting to look at the stationary distribution,

$$P_r^{\text{st}}(J_r) = r\int_0^\infty d\tau \frac{e^{-r\tau}}{\sqrt{2\pi\sigma_\tau^2}}\exp\left[-\frac{(J_r - \mu_\tau)^2}{2\sigma_\tau^2}\right], \quad (69)$$

where $\mu_\tau = \sqrt{\tau/\pi}$ and $\sigma_\tau^2 = \sqrt{\tau/\pi}(1 - 1/\sqrt{2})$ are the mean and the variance of the current in the absence of resetting, respectively. From the small and large τ asymptotic behavior of the integrand, it is easy to realize that the above integral is convergent for any given J_r. We use the series expansion of $e^{-r\tau}$ in Eq. (69) to evaluate $P_r^{\text{st}}(J_r)$ as a sum of integrals. Each integral in the sum converges due to the reason mentioned above, and we get an explicit expression for $P_r^{\text{st}}(J_r)$ as a series sum,

$$P_r^{\text{st}}(J_r) = \frac{2\sqrt{2}r}{\pi^{1/4}\sqrt{b}}\exp\left(\frac{J_r}{b}\right)$$
$$\times \sum_{n=0}^\infty \frac{(-r)^n}{n!}(\sqrt{\pi}J_r)^{2n+\frac{3}{2}}K_{2n+\frac{3}{2}}\left(\frac{J_r}{b}\right). \quad (70)$$

We here have used $b = (1 - 1/\sqrt{2})$ for brevity, and $K_\nu(z)$ is the modified Bessel function of the second kind [54] [see Eq. (10.31.1) therein]. Using Eq. (70), the stationary distribution $P_r^{\text{st}}(J_r)$ can be computed to arbitrary accuracy. This is demonstrated in Fig. 9(a) where the theoretical computation is plotted together with the simulation results.

The stationary distribution has some interesting features which are visible from Fig. 9(a). First, it is apparent that $P_r^{\text{st}}(J_r)$ is vanishingly small for negative values of J_r. This can be understood in the following way. Let us recall that, at any time, the total current is nothing but the net number
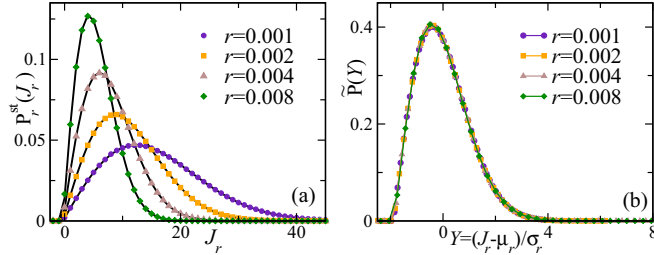
FIG. 9. Stationary probability distribution of the total current $P_r^{st}(J_r)$: (a) Plot of $P_r^{st}(J_r)$ for different (small) values of r; symbols represent the data obtained from numerical simulations, and solid lines correspond to the analytical result obtained using Eq. (70). (b) Plot of the same data as in panel (a) as a function of $Y = (J_r - \mu_r)/\sigma_r$. For simulations we have used $L = 1000$.

of particles hopping across the central bond since the last resetting event, i.e., after being brought to the configuration $\mathcal{C}_0$ where the left half of the lattice is filled up. To produce a negative current, the number of particles crossing the central bond from left to right should be lower than that from right to left, i.e., there should be a net flux of the particles to the left. Since the particles are allowed to hop only to empty neighboring sites, starting from the configuration $\mathcal{C}_0$, this is an extremely unlikely event and has a vanishingly small probability.

Second, it also appears that $P_r^{st}(J_r)$ is strongly non-Gaussian, which is manifest in the asymmetric behavior of the two tails, as seen in Fig. 9(a). To characterize this asymmetry and the non-Gaussian nature quantitatively we look at the decay of $P_r^{st}(J_r)$ at the two tails, namely, near $J_r = 0$ and large J_r. Near $J_r = 0$, for small values of r, the behavior is dominated by the $n = 0$ term in Eq. (70). One can then use the asymptotic behavior of $K_{\frac{3}{2}}(z)$ near $z = 0$ to get

$$P_r^{st}(J_r) \approx 2\pi r \left(J_r + 1 - \frac{1}{\sqrt{2}} \right) + O(r^2). \tag{71}$$

Clearly, for small values of r, the probability distribution of the total current J_r decays linearly near $J_r = 0$.

To determine how $P_r^{st}(J_r)$ decays for large J_r we use the asymptotic behavior of $K_\nu(z)$; for large values of the argument z, we have [see Ref. [54], (Eq. 10.40.2)]

$$\lim_{z \to \infty} K_\nu(z) \approx \sqrt{\frac{\pi}{2z}} e^{-z}. \tag{72}$$

Using that in Eq. (70) and performing the sum over n, we get

$$P_r^{st}(J_r) \approx 2\pi r J_r e^{-\pi r J_r^2} + O(r^2). \tag{73}$$

Note that the above expression holds true to the leading order in r, and higher order corrections can be systematically calculated by including higher order terms in (72).

We conclude the discussion about $P_r^{st}(J_r)$ with one final remark. From our numerical data, we observe a surprising collapse of the current distribution when plotted as a function of the scaled variable $Y = (J_r - \mu_r)/\sigma_r$ where μ_r and σ_r are, respectively, the mean and the variance of J_r. The collapse is shown in Fig. 9(b) where the scaled distribution $\tilde{P}(Y)$ appears to be independent of r as the curves corresponding to different values of r from Fig. 9(a) fall on top of each other.

To understand this collapse, let us look at $\tilde{P}(Y)$ predicted from Eqs. (73) and (71). Recalling that for small values of r, $\mu_r \simeq \frac{1}{2\sqrt{r}}$, and $\sigma_r \simeq \sqrt{\frac{(4-\pi)}{4\pi r}}$, we get from Eq. (73),

$$\tilde{P}(Y) \approx \frac{1}{2}[\sqrt{\pi(4-\pi)} + (4-\pi)Y]e^{-\frac{1}{4}\left(\sqrt{\pi} + \sqrt{4-\pi}Y\right)^2}$$
$$+ O(r^{3/2}). \tag{74}$$

Clearly, to the leading order in r, $\tilde{P}(Y)$ calculated from Eq. (73) (corresponding to large values of J_r) is independent of r and is consistent with the scaling collapse observed in Fig. 9(b). On the other hand, it can be easily seen that Eq. (71) does not lend itself to a similar form; $\tilde{P}(Y)$ derived from Eq. (71) depends explicitly on r,

$$\tilde{P}(Y) \approx \frac{1}{2}\sqrt{\pi(4-\pi)}\left[1 + \sqrt{\frac{4-\pi}{\pi}}Y + (2-\sqrt{2})\sqrt{r}\right]$$
$$+ O(r^{3/2}). \tag{75}$$

Hence, while for large positive J_r ($\gtrsim \mu_r + \sigma_r$), the distribution $\tilde{P}(Y)$ becomes independent of r, it is not the case in the $J_r \to 0$ limit. Indeed, as seen from Eq. (75), $\tilde{P}(Y)$ explicitly depends on r. However, notice that the r dependence in Eq. (75) comes in the form of an additional term proportional to $\sqrt{r}$, which is vanishingly small for $r \ll 1$. This makes the expected mismatch in the collapse at the left tail in Fig. 9(b) practically invisible where an apparent collapse is also observed.

V. CONCLUSION

In this article, we explore the effect of stochastic resetting on interacting many-particle systems. To this end, we study the dynamical properties of a canonical setup, namely, the symmetric exclusion process in the presence of stochastic resetting. The resetting is implemented by interrupting the dynamical evolution of the exclusion process with some rate r and restarting it from a steplike configuration where all the particles are clustered together in the left half of the system.

We find that the presence of resetting strongly affects the behavior of the system. The key findings are as follows. First, in a finite-size system, the density profile evolves to an inhomogeneous stationary profile in contrast to the flat profile in the absence of resetting. We have exactly calculated the full time-dependent density profile for arbitrary resetting rate r. Second, we find that, in a thermodynamically large system the resetting mechanism drastically changes the $\sqrt{t}$ growth of the diffusive current to linear in t. We have explicitly computed the mean and variance of the diffusive current, and the latter is also shown to have a linear growth in the long-time regime. Apart from the diffusive current, we also identify the other component of the current which arises due to the resetting move and show that this resetting current is negative, with a linear temporal growth in magnitude. The moments of the total current, i.e., the sum of the diffusive and resetting current, are also calculated using the renewal approach.

We also have investigated the probability distribution of the diffusive current J_d, resetting current J_{reset}, and the total current J_r. We have found that that while the typical fluctuations of J_d and J_{reset} are Gaussian in nature, the distribution of J_r is

strictly non-Gaussian. The non-Gaussian nature is manifest in the asymmetric asymptotic behavior of the distribution at the two tails, which we also demonstrate.

Our study opens up a new direction in the area of stochastic resetting and gives rise to a wide range of further questions. For example, it would be interesting to study the effect of stochastic resetting in other interacting particle systems, e.g., the asymmetric exclusion process, driven and equilibrium lattice gas models, etc. Furthermore, it would also be interesting to study the behavior of these interacting particle systems under various other resetting mechanisms like resetting at power-law times or time-dependent resetting, etc.

Apart from these theoretical questions, the framework of stochastic resetting in exclusion processes can also be relevant in the context of certain biophysical systems. For example, stochastic motion of backtracked RNA polymerases can be modeled as an interacting many-particle random walk on the DNA template, with RNA cleavage playing the role of resetting dynamics [14,56].

Similarly, motion of two-headed molecular motors such as kinesin and myosin V moving on a polymeric track can be modeled as an energy-driven hopping process in the presence of backward jumps (or resetting) [57]. We believe that the formalism introduced in the present work will be useful in understanding such systems.

APPENDIX A: DENSITY PROFILE OF SEPS IN THE ABSENCE OF RESETTING

In this section we present a brief account of the dynamical evolution of the density profile and current for ordinary SEPs, starting from the steplike configuration $\mathcal{C}_0$. In the absence of resetting, the time evolution of the system is governed by the free Markov matrix $\mathcal{L}_0$ which yields, for the density profile,

$$\frac{d}{dt}\rho_0(x,t) = \rho_0(x+1,t) + \rho_0(x-1,t) - 2\rho_0(x,t). \quad (A1)$$

The corresponding Fourier components $\tilde{\rho}_0(n,t)$ evolve following

$$\frac{d}{dt}\tilde{\rho}_0(n,t) = -\lambda_n \tilde{\rho}_0(n,t), \quad (A2)$$

where, as before, $\lambda_n = 2(1 - \cos\frac{2\pi n}{L})$, with $n = 0, 1, 2, \ldots, L-1$. The above equation is immediately solved to obtain

$$\tilde{\rho}_0(n,t) = e^{-\lambda_n t}\tilde{\phi}(n), \quad (A3)$$

where $\tilde{\phi}(n)$ corresponds to the initial profile $\phi(x)$. Note that $\lambda_0 = 0$, and hence $\tilde{\rho}_0(0,t) = \tilde{\phi}(0) = \frac{L}{2}$ does not evolve with time.

The spatial density profile is obtained by taking the inverse Fourier transform of Eq. (A3). In particular, for the steplike initial profile $\phi(x) = 1 - \Theta(x + 1 - \frac{L}{2})$ we have

$$\rho_0(x,t) = \frac{1}{2} + \frac{1}{L}\sum_{n=1,3}^{L-1} e^{-i\frac{2\pi nx}{L}}\left(1 + i\cot\frac{\pi n}{L}\right)e^{-\lambda_n t}. \quad (A4)$$

APPENDIX B: BEHAVIOR OF CURRENT IN THE ABSENCE OF RESETTING

In the absence of resetting the only source of current in SEPs is the hopping dynamics of the particles. The average instantaneous current across the initial step, i.e., across the central bond ($\frac{L}{2} - 1, \frac{L}{2}$), is given by

$$\langle j_0(t)\rangle = \rho_0\left(\frac{L}{2} - 1, t\right) - \rho_0\left(\frac{L}{2}, t\right) = \frac{2}{L}\sum_{n=1,3}^{L-1} e^{-\lambda_n t}, \quad (B1)$$

where we have used Eq. (A4) to calculate the average densities at the sites $x = \frac{L}{2} - 1$ and $x = \frac{L}{2}$. Clearly, in the long-time limit $t \to \infty$, the instantaneous current vanishes as the density profile becomes flat.

We are interested in the time-integrated current $J_0(t) = \int_0^t ds\, j_0(s)$, which measures the net number of particles crossing the central bond towards right. The average time-integrated current is obtained by integrating Eq. (B1),

$$\langle J_0(t)\rangle = \frac{2}{L}\sum_{n=1,3}^{L-1}\frac{1}{\lambda_n}(1 - e^{-\lambda_n t}). \quad (B2)$$

For any finite L, the average time-integrated current $J_0(t)$ saturates to an L-dependent constant value in the long-time limit.

To understand the behavior of a thermodynamically large system, one has to take the limit $L \to \infty$ first. In this case, the sum in Eq. (B1) can be converted to an integral by denoting $q = 2\pi n/L$, and we have the mean instantaneous current,

$$\langle j_0(t)\rangle = \int_0^{2\pi}\frac{dq}{2\pi}e^{-2(1-\cos q)t} = e^{-2t}I_0(2t). \quad (B3)$$

Here $I_0(x)$ is the modified Bessel function of the first kind [54] [see Eq. (10.25.2) therein]. In this limit, the average time-integrated current becomes

$$\langle J_0(t)\rangle = e^{-2t}t[I_0(2t) + I_1(2t)]. \quad (B4)$$

For large values of the argument x, both $I_0(x)$ and $I_1(x)$ have the same asymptotic behavior [see Ref. [54], Eq. (10.40.1)],

$$\lim_{x\to\infty}I_{0,1}(2x) \sim \frac{e^{2x}}{2\sqrt{\pi x}}, \quad (B5)$$

which yields, in the long-time regime,

$$\langle J_0(t)\rangle \simeq \sqrt{\frac{t}{\pi}}. \quad (B6)$$

This result has been obtained in Ref. [52], albeit using a different method. In fact, it has also been shown [52] that, in the long-time regime, all the higher moments of J_0 show a

similar behavior. In particular, the variance is given by

$$\langle J_0^2(t) \rangle - \langle J_0(t) \rangle^2 \simeq \sqrt{\frac{t}{\pi}} \left(1 - \frac{1}{\sqrt{2}} \right). \quad \text{(B7)}$$

The above equation is used in Eq. (60) to calculate $\langle J_r^2 \rangle$.

1. Probability distribution of J_0

For an ordinary SEP, the probability distribution of the time-integrated current J_0 was explored in Ref. [52]. There the authors considered a scenario where, initially, each site to the left (respectively, right) of the origin ($x \leqslant 0$ and $x > 0$ respectively) is occupied with probability ρ_a (respectively ρ_b). It was shown that, for large t, the moment-generating function of the total particle flux $J_0(t)$ through the origin is given by

$$\langle e^{\lambda J_0(t)} \rangle \sim e^{\sqrt{t} F(\omega)}, \quad \text{(B8)}$$

where $\omega = \rho_a(e^\lambda - 1) + \rho_b(e^{-\lambda} - 1) + \rho_a \rho_b(e^\lambda - 1)$ and

$$F(\omega) = \frac{1}{\sqrt{\pi}} \sum_{n=1}^{\infty} \frac{(-1)^{n+1} \omega^n}{n^{3/2}} \equiv -\frac{1}{\sqrt{\pi}} \text{PolyLog}_{3/2}(-\omega). \quad \text{(B9)}$$

In our case, we have $\rho_a = 1$ and $\rho_b = 0$ which simplifies ω and in turn $F(\omega)$; we get $\omega = e^\lambda - 1$ and

$$F(\lambda) = -\frac{1}{\sqrt{\pi}} \text{PolyLog}_{3/2}(1 - e^\lambda), \quad \text{(B10)}$$

which is quoted in Eq. (35).

It has been shown in Ref. [52] that the corresponding probability distribution $P_0(J_0, t)$, in the long-time limit, is of the form

$$P_0(J_0, t) \sim e^{\sqrt{t} G(J_0/\sqrt{t})}. \quad \text{(B11)}$$

The large deviation function $G(q = J_0/\sqrt{t})$ is related to $F(\lambda)$ through a Legendre transform,

$$G(q) = \min_\lambda [F(\lambda) - \lambda q] = F(\lambda^*) - \lambda^* q, \quad \text{(B12)}$$

where λ^* corresponds to the minimum of the function $F(\lambda) - \lambda q$ and is obtained by solving $\frac{dF(\lambda)}{d\lambda} = q$. It is easy to see that for small values of q, λ^* is also small. Hence, it is convenient to use the series expansion of $F(\lambda)$ near $\lambda = 0$,

$$F(\lambda) = \frac{\lambda}{\sqrt{\pi}} + \frac{\lambda^2}{2\sqrt{\pi}} \left(1 - \frac{1}{\sqrt{2}} \right) + O(\lambda^3), \quad \text{(B13)}$$

to find λ^* for small values of q. Restricting ourselves to the quadratic order in λ, we get $\lambda^* = \frac{(q\sqrt{\pi}-1)\sqrt{2}}{(\sqrt{2}-1)}$. Substitution of
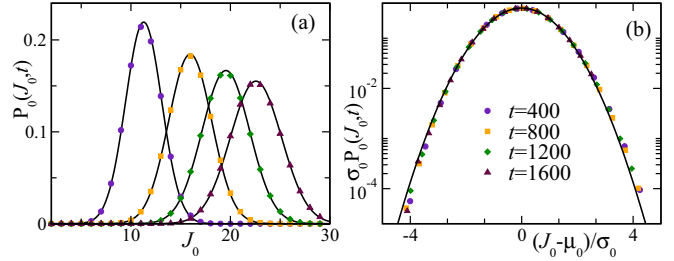
FIG. 10. (a) Plot of $P_0(J_0, t)$ vs J_0 for different (large) values of t. The symbols indicate the data obtained from numerical simulation of a system of size $L = 1000$, whereas the solid black lines correspond to the Gaussian distribution [see Eq. (B15)]. (b) The same data plotted as function of $[J_0 - \mu_0(t)]/\sigma_0(t)$; the solid line indicates the standard normal distribution.

this λ^* in Eq. (B12) yields

$$G(q) = \frac{\left(q - \frac{1}{\sqrt{\pi}} \right)^2}{\frac{2}{\sqrt{\pi}} \left(1 - \frac{1}{\sqrt{2}} \right)}. \quad \text{(B14)}$$

Using the above $G(q)$ in Eq. (B11) results in a Gaussian form for the current distribution,

$$P_0(J_0, t) = \frac{1}{\sqrt{2\pi \sigma_0^2(t)}} \exp \left\{ -\frac{[J_0 - \mu_0(t)]^2}{2\sigma_0^2(t)} \right\}, \quad \text{(B15)}$$

where the prefactor is just a normalization constant. Here $\mu_0(t) = \sqrt{\frac{t}{\pi}}$ is nothing but the average hopping current $\langle J_0(t) \rangle$ and $\sigma_0^2(t) = \sqrt{\frac{t}{\pi}}(1 - \frac{1}{\sqrt{2}})$ is the variance [see Eq. (B7)]. Note that this Gaussian distribution is expected only in the long-time limit, as Eq. (B11) holds true in this limit only.

Figure 10(a) shows a comparison of $P_0(J_0, t)$ obtained from numerical simulations (symbols) with the that predicted from Eq. (B15) (solid lines) for different (large) values of t. Figure 10(b) shows the same data but plotted against the scaled variable $y = \frac{J_0 - \mu_0(t)}{\sigma_0(t)}$; the solid line corresponds to the standard normal distribution $\frac{1}{\sqrt{2\pi}} e^{-y^2/2}$. The numerical data show a very good match with the predicted Gaussian curve for typical values of J_0; there are deviations only at the regime $|y| \gg 1$, which are visible only at a logarithmic scale. The large deviation function calculated in Ref. [52] describes the distribution for these atypical values. However, as shown in Sec. IV C, for our purposes it suffices to consider the typical fluctuations, and we use the Gaussian distribution (B15) to calculate the distribution of the diffusive current J_d in the presence of resetting.

[1] O. Bénichou, C. Loverdo, M. Moreau, and R. Voituriez, Rev. Mod. Phys. **83**, 81 (2011).

[2] A. Chechkin and I. M. Sokolov, Phys. Rev. Lett. **121**, 050601 (2018).

[3] A. Pal and S. Reuveni, Phys. Rev. Lett. **118**, 030603 (2017).

[4] A. Pal, Ł. Kuśmierz, and S. Reuveni, arXiv:1906.06987.

[5] S. C. Manrubia and D. H. Zanette, Phys. Rev. E **59**, 4945 (1999).

[6] P. Visco, R. J. Allen, S. N. Majundar, and M. R. Evans, Biophys. J. **98**, 1099 (2010).

[7] T. Rotbart, S. Reuveni, and M. Urbakh, Phys. Rev. E **92**, 060101(R) (2015).

[8] S. Reuveni, M. Urbakh, and J. Klafter, Proc. Natl. Acad. Sci. USA **111**, 4391 (2014).

[9] A. Montanari and R. Zecchina, Phys. Rev. Lett. **88**, 178701 (2002).

[10] L. Lovasz, in *Combinatronics*, Vol. 2 (Bolyai Society for Mathematical Studies, Budapest, 1996), p. 1.

[11] D. Sornette, Phys. Rep. **378**, 1 (2003); *Why Stock Markets Crash* (Princeton University Press, Princeton, NJ, 2017).

[12] E. Kussell and S. Leiber, Science **309**, 2075 (2005).

[13] E. Kussell, R. Kishony, N. Q. Balaban, and S. Leiber, Genetics **169**, 1807 (2005).

[14] E. Roldán, A. Lisica, D. Sánchez-Taltavull, and S. W. Grill, Phys. Rev. E **93**, 062411 (2016).

[15] M. R. Evans and S. N. Majumdar, Phys. Rev. Lett. **106**, 160601 (2011).

[16] M. R. Evans and S. N. Majumdar, J. Phys. A **44**, 435001 (2011).

[17] M. R. Evans, S. N. Majumdar, and K. Mallick, J. Phys. A **46**, 185001 (2013).

[18] J. Whitehouse, M. R. Evans, and S. N. Majumdar, Phys. Rev. E **87**, 022118 (2013).

[19] M. R. Evans and S. N. Majumdar, J. Phys. A **47**, 285001 (2014).

[20] V. Méndez and D. Campos, Phys. Rev. E **93**, 022106 (2016).

[21] A. Masó-Puigdellosas, D. Campos, and V. Méndez, Phys. Rev. E **99**, 012141 (2019).

[22] D. Gupta, J. Stat. Mech. (2019) 033212.

[23] A. Pal, R. Chatterjee, S. Reuveni, and A. Kundu, J. Phys. A **52**, 264002 (2019).

[24] A. Pal, Phys. Rev. E **91**, 012113 (2015).

[25] S. Ahmad, I. Nayak, A. Bansal, A. Nandi, and D. Das, Phys. Rev. E **99**, 022130 (2019).

[26] A. Chatterjee, C. Christou, and A. Schadschneider, Phys. Rev. E **97**, 062106 (2018).

[27] A. Pal and V. V. Prasad, Phys. Rev. E **99**, 032123 (2019).

[28] M. Basu, P. K. Mohanty, Europhys. Lett. **90**, 50005 (2010).

[29] D. Boyer and C. Solis-Salas, Phys. Rev. Lett. **112**, 240601 (2014).

[30] S. N. Majumdar, S. Sabhapandit, and G. Schehr, Phys. Rev. E **92**, 052126 (2015).

[31] Ł. Kuśmierz, S. N. Majumdar, S. Sabhapandit, and G. Schehr, Phys. Rev. Lett. **113**, 220602 (2014).

[32] X. Durang, M. Henkel, and H. Park, J. Phys. A **47**, 045002 (2014).

[33] J. Masoliver, Phys. Rev. E **99**, 012121 (2019).

[34] M. R. Evans and S. N. Majumdar, J. Phys. A **51**, 475003 (2018).

[35] C. Maes and T. Thiery, J. Phys. A **50**, 415001 (2017).

[36] U. Bhat, C. De Bacco, and S. Redner, J. Stat. Mech. (2016) 083401.

[37] E. Roldán and S. Gupta, Phys. Rev. E **96**, 022130 (2017).

[38] A. Pal and A. Kundu, and M. R. Evans, J. Phys. A **49**, 225001 (2016).

[39] V. P. Shkilev, Phys. Rev. E **96**, 012126 (2017).

[40] M. R. Evans and S. N. Majumdar, J. Phys. A **52**, 01LT01 (2019).

[41] A. Masó-Puigdellosas, D. Campos, and V. Méndez, J. Stat. Mech. (2019) 033201.

[42] A. Nagar and S. Gupta, Phys. Rev. E **93**, 060102(R) (2016).

[43] S. Eule and J. J. Metzger, New J. Phys. **18**, 033006 (2016).

[44] A. S. Bodrova, A. V. Chechkin, and I. M. Sokolov, Phys. Rev. E **100**, 012120 (2019); **100**, 012119 (2019).

[45] R. Falcao and M. R. Evans, J. Stat. Mech. (2017) 023204.

[46] S. Gupta, S. N. Majumdar, and G. Schehr, Phys. Rev. Lett. **112**, 220601 (2014).

[47] S. Gupta and A. Nagar, J. Phys. A **49**, 445001 (2016).

[48] B. Mukherjee, K. Sengupta, and S. N. Majumdar, Phys. Rev. B **98**, 104309 (2018).

[49] T. T. da Silva and M. D. Fragoso, J. Phys. A **51**, 505002 (2018).

[50] T. Liggett, *Interacting Particle Systems* (Springer-Verlag, Berlin, 1985).

[51] F. Spitzer, Adv. Math. **5**, 246 (1970).

[52] B. Derrida and A. Gerschenfeld, J. Stat. Phys. **136**, 1 (2009).

[53] B. Derrida, B. Douçot, and P.-E. Roche, J. Stat. Phys. **115**, 717 (2004).

[54] F. W. J. Olver, A. B. Olde Daalhuis, D. W. Lozier, B. I. Schneider, R. F. Boisvert, C. W. Clark, B. R. Miller, and B. V. Saunders (eds.), NIST Digital Library of Mathematical Functions, https://dlmf.nist.gov/.

[55] Of course, the time durations $\{t_i\}$ are different.

[56] A. Lisica, C. Engel, M. Jahnel, E. Roldán, E. A. Galburt, P. Cramer, and S. W. Grill, Proc. Natl. Acad. Sci. USA **113**, 2946 (2016).

[57] R. D. Astumian, Biophys. J. **98**, 2401 (2010).